RESEARCH ARTICLE

Macromolecular Bioscience

www.mbs-journal.de

Physicochemical Characterization of Pectin-Gelatin Biomaterial Formulations for 3D Bioprinting

Anna Lapomarda, Giorgia Cerqueni, Mike A. Geven, Irene Chiesa, Aurora De Acutis, Matteo De Blasi, Francesca Montemurro, Carmelo De Maria, Monica Mattioli-Belmonte, and Giovanni Vozzi*

Developing biomaterial formulations with specific biochemical characteristics and physical properties suitable for bioprinting of 3D scaffolds is a pivotal challenge in tissue engineering. Therefore, the design of novel bioprintable formulations is a continuously evolving research field. In this work, the authors aim at expanding the library of biomaterial inks by blending two natural biopolymers: pectin and gelatin. Cytocompatible formulations are obtained by combining pectin and gelatin at different ratios and using (3-glycidyloxypropyl)trimethoxysilane (GPTMS) as single crosslinking agent. It is shown that the developed formulations are all suitable for extrusion-based 3D bioprinting. Self-supporting scaffolds with a designed macroporosity and micropores in the bioprinted struts are successfully obtained by combining extrusion-based bioprinting and freeze-drying. The presence of gelatin in these formulations allows for the modulation of porosity, of water uptake and of scaffold stiffness in respect to pure pectin scaffolds. Results demonstrate that these new biomaterial formulations, processed with this specific approach, are promising candidates for the fabrication of tissue-like scaffolds for tissue regeneration.

1. Introduction

Fabrication of scaffolds by 3D bioprinting is gaining increasing attention to replace, restore, or regenerate defective tissues.[1,2] The ability to reproduce the complex anatomical features of targeted tissues through automated technologies is what makes this biofabrication approach unique.[1] Differently from conventional fabrication techniques (such as salt leaching, solvent casting), 3D bioprinting ensures spatial and temporal control of the complete biofabrication process. Additionally, the use of 3D bioprinting allows for the production of well-defined patient-specific implants with tunable degree of porosity and architecture.[3–6]

Extrusion-based bioprinting is one of the most used bioprinting technology for producing tissue-like scaffolds due to its versatility and user-friendliness. The ability to easily change processing parameters (e.g., flow rate, bioprinting speed) or hardware components (e.g., shape and size of the extrusion tip), and to work under different operative conditions (e.g., aseptic and physiological conditions) enables extrusion-based bioprinting to process a broad range of biomaterial inks and bioinks.[1,2] However, developing biocompatible and cell-friendly biomaterial formulations with specific physicochemical properties suitable for bioprinting, still remains one of the most challenging aspects that limits the spreading of this bioprinting technology in a clinical setting.[4,7]

A multitude of biomaterials has been explored to form printable formulations both for bioinks and biomaterial inks. In this respect, hydrogels are the most prominent class of biomaterials

A. Lapomarda, I. Chiesa, Dr. A. De Acutis, Dr. F. Montemurro, Dr. C. De Maria, Prof. G. Vozzi
Research Center 'E. Piaggio'
University of Pisa
Via Diotisalvi, 1, Pisa 56122, Italy
E-mail: anna.lapomarda@ing.unipi.it

The ORCID identification number(s) for the author(s) of this article can be found under https://doi.org/10.1002/mabi.202100168

DOI: 10.1002/mabi.202100168

A. Lapomarda, I. Chiesa, M. De Blasi, Dr. C. De Maria, Prof. G. Vozzi
Department of Ingegneria dell'Informazione
University of Pisa
Via Girolamo Caruso, 16, Pisa 56122, Italy

G. Cerqueni, Prof. M. Mattioli-Belmonte
Department of Scienze Cliniche e Molecolari
Università Politecnica delle Marche
Via Tronto 10/A, Ancona 60121, Italy

Dr. M. A. Geven
Laboratory of Polymers and Biomaterials
Istituto Italiano di Tecnologia
Via Morego 30, Genova 16163, Italy

for tissue engineering (TE) applications.[4,8–10] These highly hydrated polymeric networks are able to mimic many features of the natural extracellular matrix. They provide a viable engineered microenvironment for cell adhesion, growth and proliferation. However, their rheological properties often limit their use for bioprinting of scaffolds with complex shapes. Their low viscosity and yield stress may, in fact, result in premature collapse of bioprinted scaffolds over time under their own weight. Therefore, only simple and bidimensional bioprinted structures with poor shape fidelity are often obtained with these materials.[11–14]

Various synthetic (e.g., polyethylene glycol) and natural (gelatin, hyaluronic acid, alginate) polymers, as well as their combinations have been exploited for bioprinting of hydrogel scaffolds.[4,8] More recently, pectin-based hydrogels have gained attention for the formulation of green and sustainable biomaterial inks[3] and bioinks[15] for extrusion-based bioprinting. Pectin is a biocompatible and naturally occurring biopolymer that commonly constitutes the tissues of most plants.[16] It is commercially derived from citrus peels and apple pomace, both by-products of food manufacturing industry. Its great gelling capability, biocompatibility, easily tunable physical properties and low-cost make pectin a valid alternative to commercial petroleum-based biopolymers.[17,18] Although pectin shows numerous advantageous properties for use as biomaterial, its inadequate rheological properties (e.g., low viscosity and yield stress)[19,20] limit its current use in bioprinting. Furthermore, the most common pectin crosslinking process is based on the use of divalent cations (e.g., Ca^{2+}), which often requires further post-printing treatments as, for example, incubation of the 3D printed scaffold in a crosslinker solution to further stabilize it.[11,15] This can affect the resolution and therefore the reproducibility and dimensional accuracy of the 3D printed scaffold. Collapsed scaffolds with poor shape fidelity are often obtained with this approach.[11] Moreover, these treatments do not allow for a fine control of network formation throughout the scaffold.[21] In our previous work, we reported on the improvement of pectin bioprintability by using (3-Glycidyloxypropyl)trimethoxysilane (GPTMS) as pectin crosslinking agent for the first time. Through a pre-crosslinking reaction with GPTMS, an increment of the viscosity and yield stress of pectin solutions by respectively 40 and 6 times was achieved. This makes pectin suitable for bioprinting complex-shaped 3D scaffolds with high shape fidelity and interconnected mesopores without the need for any additional post-printing incubation in crosslinker solutions.[3] Here, we aim to extend the biofabrication approach developed in our previous work by blending pectin with gelatin, and using GPTMS as only crosslinking agent. We hypothesize that blending gelatin with pectin may modulate the properties of the resulting pectin-based material and expand its application into the bioprinting field. As pectin, gelatin is a sustainable biopolymer that is produced from the denaturation of animal-derived collagen. Gelatin is widely used in TE applications due to its appealing features that include i) bioactivity, ii) versatility in terms of chemical modification, due to the abundance of functional groups on its polymer chain, iii) compatibility with other biopolymers, and iv) low cost.[22] We hypothesize that the combination of these two natural biopolymers may lead to pectin-based biomaterials and bioprintable formulations with tunable properties. Other works have been published on pectin-gelatin coacervation systems for TE application. [23–25] These formulations have been mainly used to produce films,[23] microspheres,[26] injectable microparticles[27] and micro-porous cylindrical scaffolds.[24]

In this work, the preparation of mesoporous pectin-gelatin scaffolds crosslinked with GPTMS (hereafter called "PectGel") is reported. A similar approach was used in our previous work,[3] to prepare and characterize pectin sponges crosslinked with GPTMS. The effect of gelatin content on porosity, pore size, water uptake and compressive modulus were initially investigated on freeze-dried PectGel sponges. Furthermore, the cytocompatibility of PectGel formulations was studied using human MG-63 osteoblast-like cells. Finally, the bioprinting capability of the developed PectGel formulations was assessed by 3D bioprinting self-supporting woodpile scaffolds with interconnected macroporosity.

2. Results and Discussion

2.1. Physicochemical Characterization of PectGel Formulations and Sponges

The chemical composition of PectGel formulations was investigated by Attenuated Total Reflectance Infrared Spectroscopy (ATR-IR). **Figure 1**A shows the ATR-IR spectra of PectGel1, PectGel2 and PectGel3 together with and GPTMS-crosslinked pectin (Pect) and gelatin (GEL) (see **Table 1**).

The ATR-IR spectrum of Pect shows the characteristic peaks of the methyl ester groups (—$COOCH_3$) and of carboxyl acid groups (—COOH) of pectin at 1730 cm^{-1} and 1620 cm^{-1}, respectively.[31] The ATR-IR spectrum of gelatin crosslinked with GPTMS (GEL) displays the characteristic peaks at 1630 cm^{-1}, 1530 cm^{-1} and 1230 cm^{-1} corresponding to amide I (C═O stretching), amide II (N—H bending) and amide III (C—N stretching), respectively.[32] Compared to Pect, the introduction of gelatin in PectGel films results in the appearance of the peak at 1530 cm^{-1}. Furthermore, the change in ratio between the peaks at 1730 and 1620 cm^{-1} is representative for the higher gelatin concentration in the films going from the PectGel1 to the PectGel3 formulation. Finally, all the presented films show the broad band (≈1160–960 cm^{-1}) and the peak at ≈905 cm^{-1} which correspond to Si—O—Si and Si—OH bonds. This confirmed that the crosslinking of gelatin and pectin by GPTMS successfully occurred.[33] Although these results are not conclusive for the type of crosslinking reactions that occur, we hypothesize that the crosslinking occurs as in Figure 1B.

Microporous sponges were obtained by freeze-drying PectGel formulations (**Figure 2**). The morphology and architecture of micropores in Pect and PectGel sponges are typical of sponges prepared by freeze-drying.[24,33] All sponges showed an intricate and interconnected network of micropores both on the surface and in the cross-section (Figure 2B.2,B.3, C.2,C.3,D.2,D.3,E.1,E.3). Particularly, PectGel1 and PectGel2 sponges are characterized by channel-like micropores oriented along all directions. These micropores are interconnected through smaller micropores with thinner walls and diameters. In PectGel3 sponges, micropores are more homogenously distributed throughout the sponge volume. The average pore size and pore size range of PectGel and

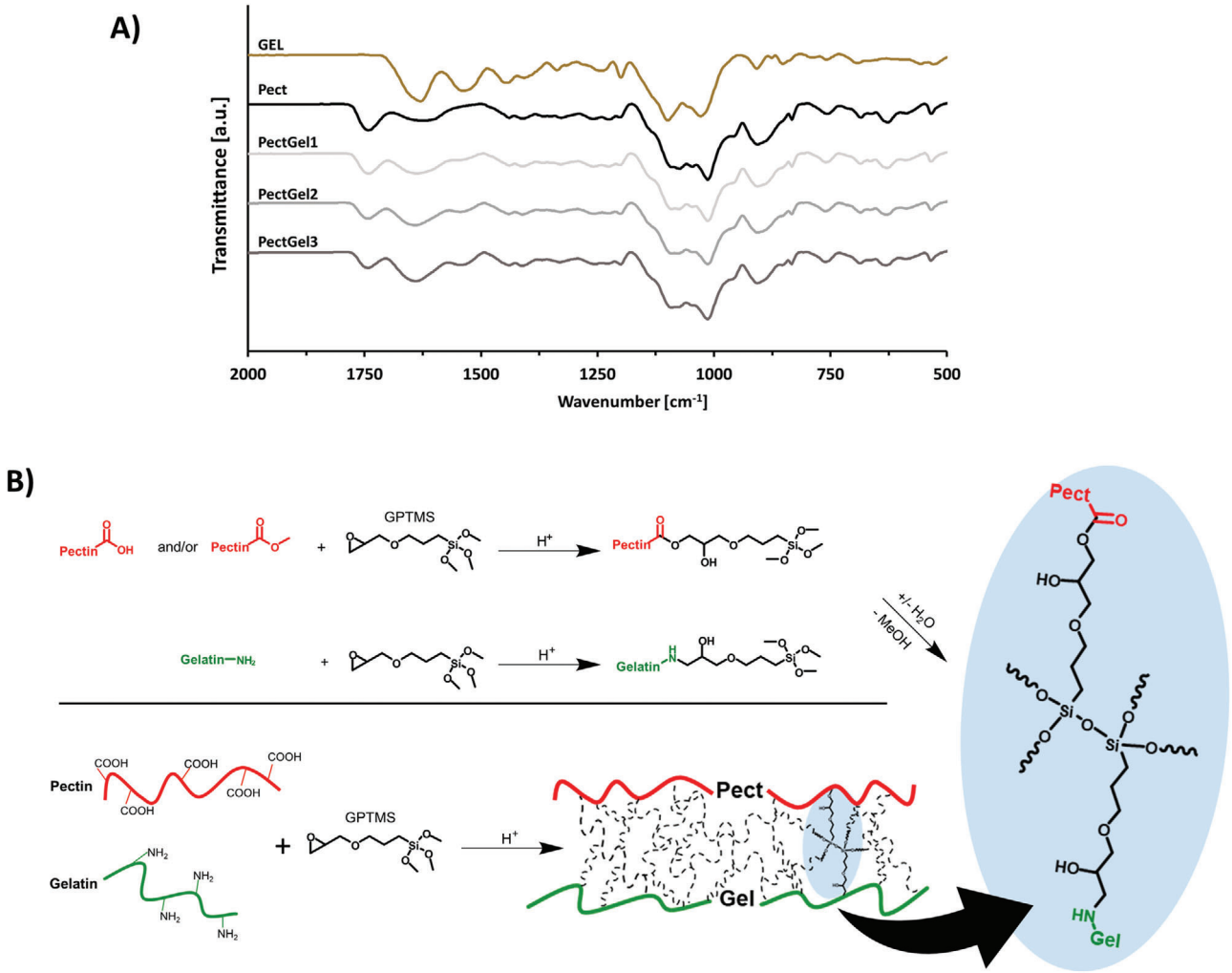

Figure 1. A) ATR-IR spectra of PectGel1, PectGel2 and PectGel3, Pect and GEL. B) Hypothetical crosslinking reaction mechanism in an aqueous environment; in an acidic environment, as generated by pectin, the GPTMS epoxide ring is opened and the resulting hydroxyl groups react with the carbonyl groups of pectin.[3] Concomitantly, an acid-catalyzed epoxide ring-opening occurs by primary amines on gelatin.[28,29] The two reactions lead to GPTMS residues linked by esters to pectin and linked by secondary amines to gelatin. Subsequently, in an aqueous environment, hydrolysis of the trimethoxysilane groups occurs (expulsion of methanol) followed by a condensation reaction forming Si-O-Si-linkages between polymer chains.[30] It must be noted that the reactions linking GPTMS to both polymers occur simultaneously in our system and are likely to compete. Which reaction is dominant and whether one of the reaction products is formed in majority is still under investigation.

Table 1. Composition of aqueous PectGel biomaterial formulations.

Name	Composition	
	Pectin [% w/v]	Gelatin [% w/v]
Pect	4	0
PectGel1	4	0.5
PectGel2	4	1
PectGel3	4	2

Pect sponges are summarized in **Table 2** together with porosity, water uptake and compressive modulus. Pect sponges showed an average pore size of 65 µm with a range of 17–123 µm, comparable to the results obtained in our previous work.[3] PectGel sponges showed larger micropores than Pect sponges, and these micropores become smaller with increasing gelatin content (Table 2).

The porosity of PectGel sponges was calculated gravimetrically. The addition of gelatin resulted in a decrease of porosity from 93.0 ± 0.2% for Pect to 89.3 ± 0.5% for PectGel3 sponges ($p < 0.0001$) (Table 2). All the sponges showed high values of porosity which are suitable for TE applications.[34]

Water uptake of Pect and PectGel sponges over time is shown in **Figure 3**A. All sponges reached an equilibrium in water uptake after 24 h. At this time point, the equilibrium water uptake seems to decrease with gelatin content (r- = −0.99) (Figure 3B, Table 2). Despite Pect sponges present the smallest pore size, these were characterized by the highest values of water uptake after 24 h (approximately two times higher than PectGel3 with the highest content of gelatin and GPTMS). We hypothesize that

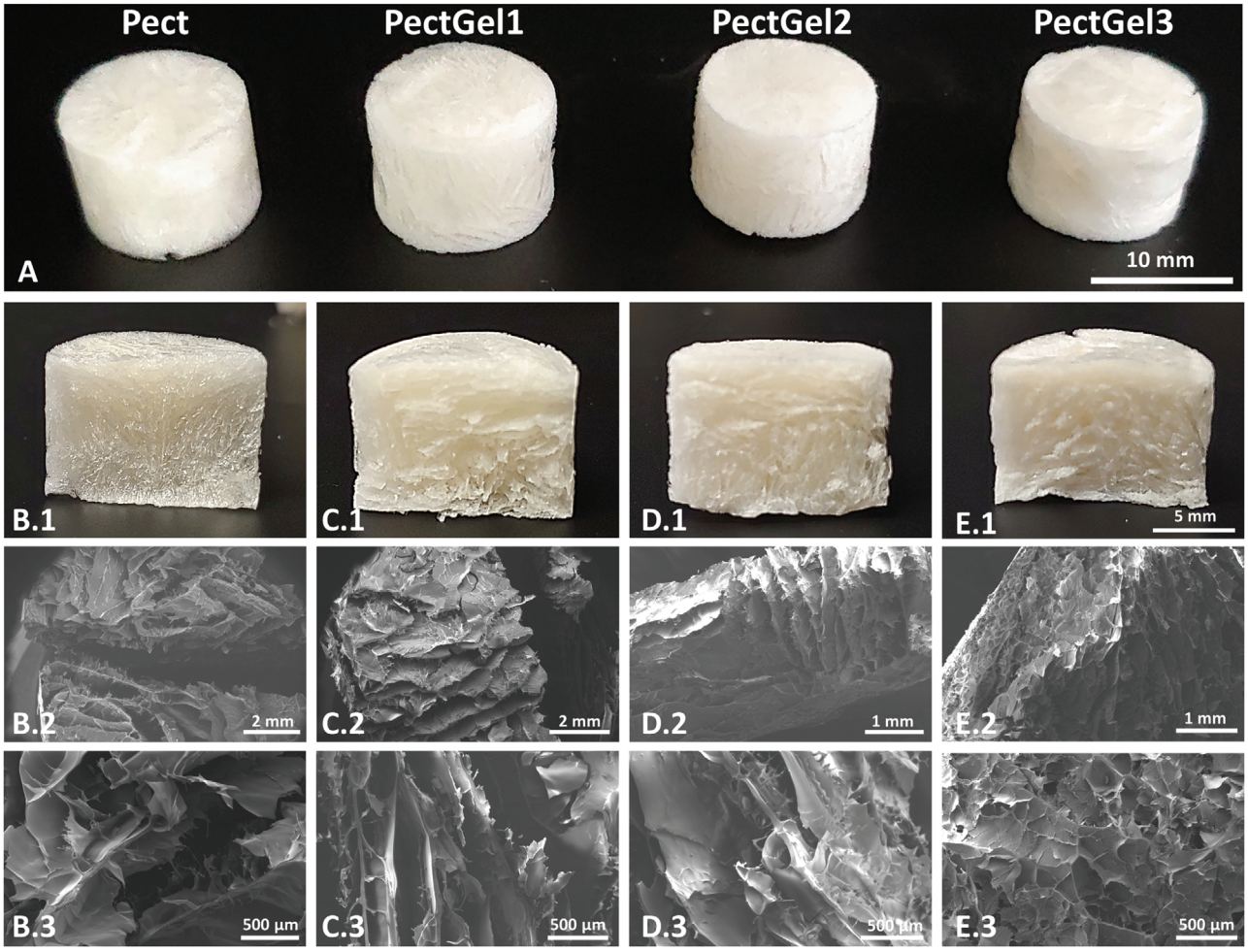

Figure 2. Images with top (A) and cross-sectional view (B.1, C.1, D.1, E.1) of Pect (B.1), PectGel1 (C.1), PectGel2 (D.1), and PectGel3 (E.1) freeze-dried sponges. Scanning Electron Microscopy (SEM) images of Pect (B.2, B.3), PectGel1 (C.2, C.3), PectGel2 (D.2, D.3), and PectGel3 (E.2, E.3) freeze-dried sponges (scale bars A = 10 mm, B.1, C.1, D.1, E.1 = 5 mm, B.2, C.2 = 2 mm, D.2, E.2 = 1mm, B.3, C.3, D.3, E.3 = 500 µm).

Table 2. Properties of microporous Pect and PectGel sponges.

Properties	Microporous sponges			
	Pect	PectGel1	PectGel2	PectGel3
Porosity [%]	93.0 ± 0.2	92.0 ± 0.1	90.9 ± 0.1	89.3 ± 0.5
Average pore size [µm]	65.0	372.0	165.8	119.9
Range of pore size [µm]	17–123	140–560	30–365	35–310
Water uptake [%]	726.2 ± 60.2	597.2 ± 12.2	563.9 ± 20.0	384.1 ± 20.3
Dry compressive modulus [kPa]	3216.8 ± 818.8	867.5 ± 214.2	1815.5 ± 460.0	4118.2 ± 370.7
Wet compressive modulus [kPa]	279.8 ± 62.0	152.7 ± 21.4	322.2 ± 72.1	370.7 ± 43.8

this behavior may be due to the higher GPTMS content needed to crosslink both pectin and gelatin.[33] The presence of siloxane chains derived from the GPTMS-mediated crosslinking reaction may, in fact, have enhanced the hydrophobicity of the PectGel sponges. The linear decrease of water uptake with gelatin (and GPTMS) supports this hypothesis.

The mechanical properties of PectGel sponges were determined by uniaxial compression test both in wet and dry conditions. Representative stress–strain curves of Pect and PectGel sponges in both testing conditions are shown in Figure 3C. Stress–strain curves of all sponges showed a linear region at low levels of stress, followed by failure of the sponges. The

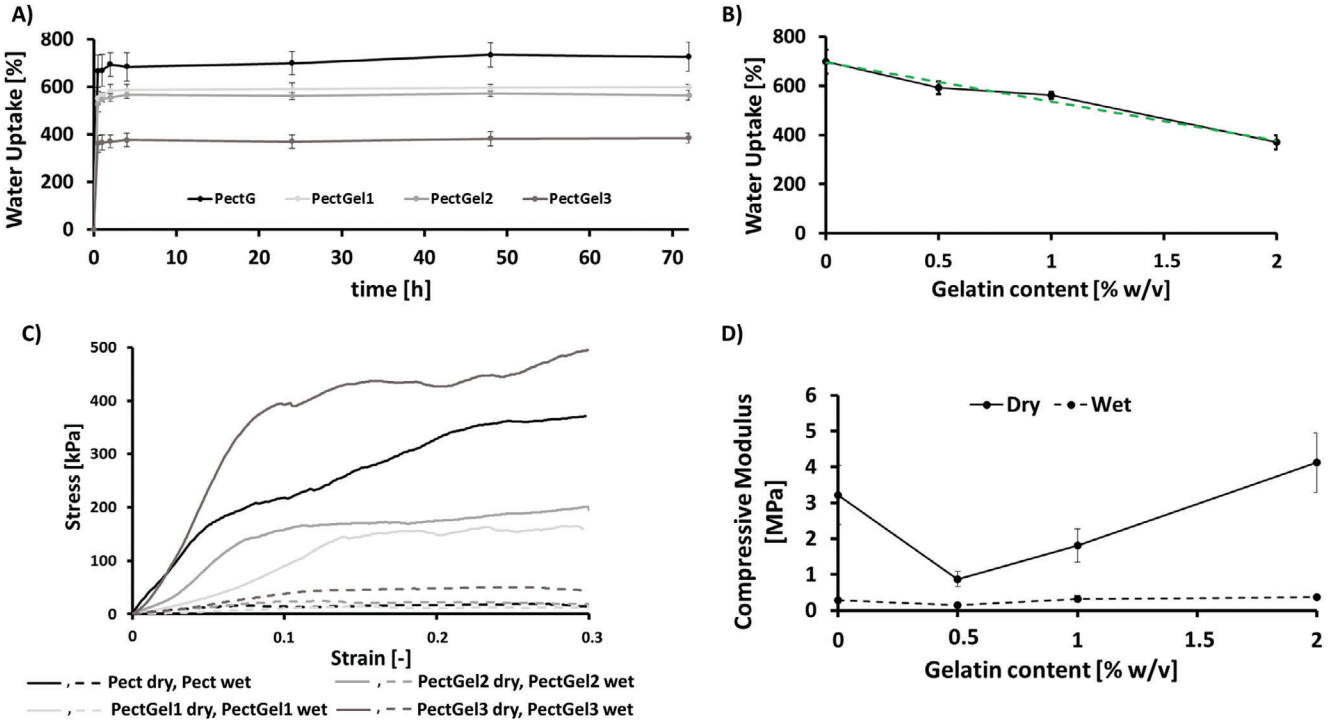

Figure 3. Water uptake profile of PectGel and PectG sponges when soaked in ultrapure water up to 3 days (A), effect of gelatin content on water uptake at 24 h (The dashed green line represents the best linear fitting of the water uptake measurements at 24 h (B), representative stress–strain curves of PectGel and Pect sponges in dry (continuous line) and wet (dashed line) conditions (C), and effect of gelatin on compressive modulus in dry (continuous line) and wet (dashed line) conditions (D).

compressive modulus in dry and wet conditions was calculated from the slope of the linear region (1–7% strain) (Table 2). As expected, the hydration of the sponges resulted in a reduction of the compressive modulus of one order of magnitude (Figure 3D). Compared to Pect sponges, the introduction of gelatin at a low concentration seems to reduce the stiffness of the sponges in dry conditions. In particular, in the dry state PectGel1 sponges shows a compressive modulus 3.7 times lower than Pect sponges ($p < 0.005$). No significant difference in stiffness was observed between PectGel2 or PectGel3 and Pect sponges, respectively. Interestingly, a linear increase of stiffness ($r = 0.99$) from PectGel1 to PectGel3 was observed. In the hydrated state, this trend is less pronounced ($r = 0.88$). Nonetheless, PectGel1 sponges demonstrated the lowest stiffness in the wet state (1.8 times lower than Pect, $p < 0.005$) as well, and PectGel3 sponges showed the highest stiffness (1.3 times higher than Pect). Conversely, hydrated PectGel2 sponges showed similar stiffness to Pect sponges. The reduction of the stiffness at low gelatin content may be attributed to a lower degree of crystallinity due to the introduction of gelatin within the pectin matrix.[23] The addition of gelatin, in fact, may cause the disruption of pectin crystalline regions, which in turn results in a decrease of the stiffness of PectGel1 and PectGel2 sponges (with low gelatin content). We hypothesize that at higher gelatin concentration this effect might be compensated by the contextual addition of GPTMS whose internal network made of covalent bonds between pectin and gelatin, and the formation of a silicate network contributed to the increasing stiffness of the sponge.

2.2. Cytocompatibility Investigation

Cytotoxicity of the developed PectGel materials was investigated by determination of MG-63 metabolic activity at 48 h through an XTT assay. Pect sponges were used as control. As can be seen in **Figure 4**A, no significant difference in cell viability was observed on PectGel1 and PectGel2 sponges compared with that of Pect sponges. While a reduction of cell viability of about 42% was observed on PectGel3 sponges. This may be due to the increased content of GPTMS which may have reduced cell adhesion on the sponge surface.[33]

Cell behavior of MG-63 cells on PectGel sponges was investigated by SEM morphological observations. Figure 4B shows representative SEM images of adherent cells on the surface of Pect and PectGel sponges at 48 h. MG-63 cells exhibited a star-like shape on all the sponges which is typical of adherent osteoblast-like cells. In particular, MG-63 cells on PectGel3 were mainly elongated or extremely flattened, features that are characteristic of viable cells.

2.3. Extrusion-Based Bioprinting of PectGel Scaffolds

PectGel and Pect biomaterial inks were obtained by mixing PectGel slurries at 70 °C until a visible increment of viscosity was observed. This increment was due to the heat-induced pre-crosslinking reaction of pectin and gelatin by GPTMS. The time required to make the formulations printable is shown

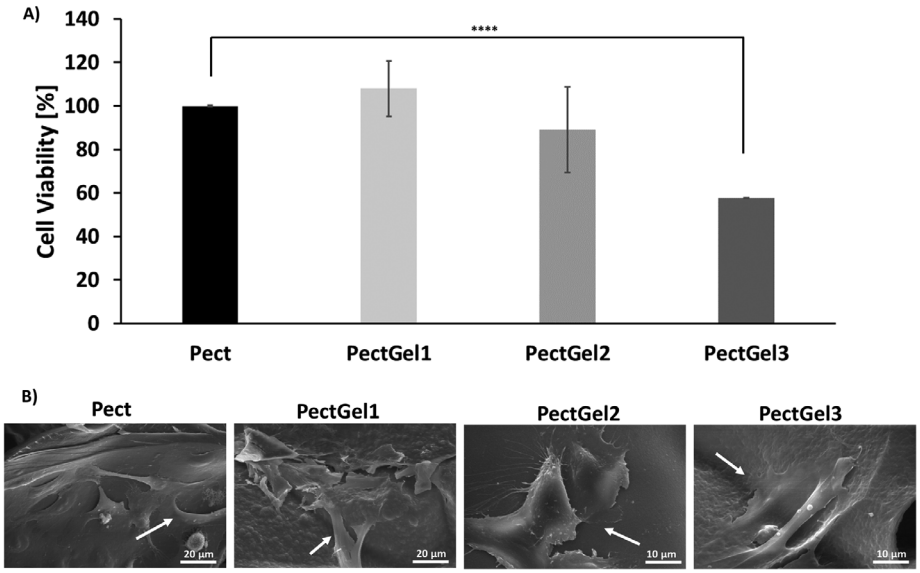

Figure 4. Cell viability at 48 h of MG-63 cells seeded on PectGel1, PectGel2, PectGel3, and PectG sponges. ("*" represents Student's *t*-test significant difference between cell viability of Pect (control) and other PectGel sponges, ****$p < 0.0001$) (A), and representative SEM images of adherent MG-63 cells on Pect and PectGel sponges at 48 h (Scale bar: Pect, PectGel1 = 20 µm; PectGel2, PectGel3 = 10 µm).

Table 3. Bioprinting parameters applied for 3D extrusion based bioprinting of Pect, PectGel1, PectGel2, and PectGel3 biomaterial inks.

Bioprinting parameters	Biomaterial inks			
	Pect	PectGel1	PectGel2	PectGel3
Time needed to induce an increment of viscosity [h]	4	3	2.5	2.5
Window of printability [h]	≈3	≈5	≈7	≈24
Bioprinting temperature [°C]	25	25	25	25
Type and size of the extrusion tip	Straight22 G	Straight22 G	Straight22 G	Straight22 G
Flow rate[a)] [%]	360	370	340	320
Printing speed [mm s^{-1}]	8	8	8	8

[a)] Flow rate values set in the G-code with respect to the nominal value calculated automatically by the slicing program Slic3r.

in **Table 3**. Following this mixing time, homogenous and uniform fibers were obtained when extruding the resulting slurry from 22 G (410 µm inner diameter) extrusion tips (**Figure 5**.A.1,B.1,C.1,D.1). Conversely, at times inferior to those reported, only droplets were formed during extrusion and no filament formation was observed. This indicated that the formulation was not yet ready to be bioprinted since the formulation was not sufficiently crosslinked. As expected, prolonged exposure to 70 °C resulted in over-crosslinking which prohibited the bioprinting, because the formulation was in a gel-like state and practically impossible to extrude. Moreover, with an increasing gelatin content, a faster viscosity increase was observed.

Once PectGel formulations were considered ready-to-bioprint, woodpile scaffolds were bioprinted in order to assess the capability of these formulations to produce self-supporting 3D structures with interconnected designed macropores. Self-standing woodpile scaffolds were successfully obtained with all PectGel biomaterial inks (Figure 5A.2,B.2,C.2,D.2). Open and interconnected macropores and no collapsed fibers were observed in all PectGel scaffolds. No distortion of the scaffolds was observed after freeze-drying (required step to complete GPTMS crosslinking reaction) and complete rehydration in ultrapure water at 37 °C (Figure 5A.3–A.7,B.3–B.7,C.3–C.7,D.3–D.7). Notably, as already shown in our previous work,[3] the freeze-drying process introduced an interconnected network of micropores within the macroporous, 3D bioprinted matrix. This is an important result since this approach allowed to further increase the final porosity of the scaffold, which in turn promotes scaffold colonization and nutrient/metabolites exchange. The sizes of micro- and macropores of the bioprinted scaffolds are summarized in Table S1, Supporting information.

Overall, these results clearly show that the addition of gelatin did not negatively affect the bioprinting capability of pectin. Interestingly, the window of printability, namely the period of time during which the formulations are suitable for bioprinting before becoming too stiff for extrusion, varied with gelatin content (see Table 3). This parameter increased with gelatin concentration, and with the GPTMS content necessary to crosslink

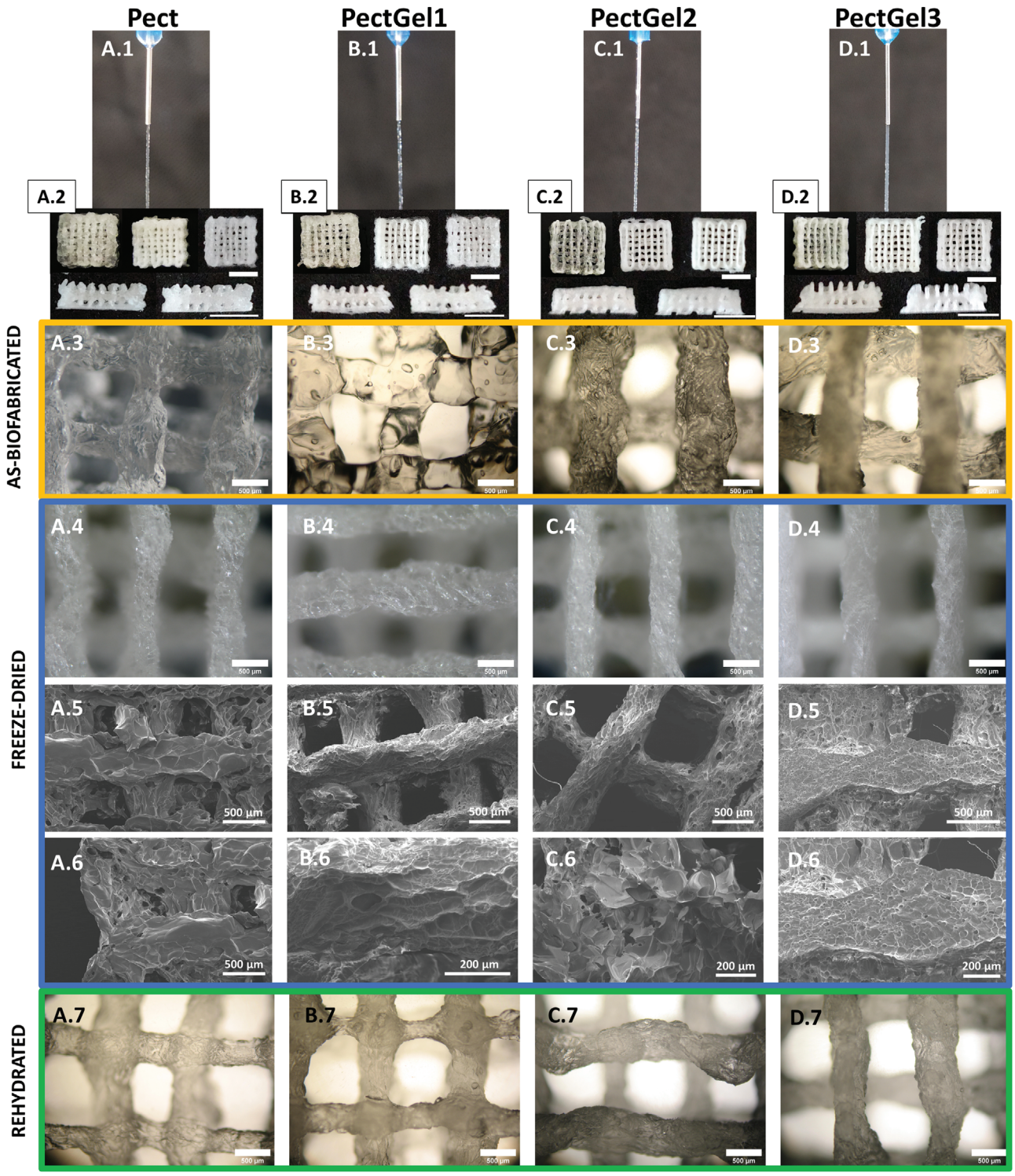

Figure 5. Images of the initial bioprinting screening to evaluate fiber formation of Pect (A.1), PectGel1 (B.1), PectGel2 (C.1), and PectGel3 (D.1) inks; top (first row) and cross-sectional views (second row) of 3D bioprinted woodpile scaffolds after bioprinting, after freeze drying and after rehydration (from left to right, respectively; note the cross-sectional image after bioprinting is not provided, being the cut a destructive operation for the gel structure) made of Pect (A.2), PectGel1 (B.2), PectGel2 (C.2) and PectGel3 (D.2). Optical microscopy images with top view of Pect (A.3, A.4, A.6), PectGel1 (B.3, B.4, B.6), PectGel2 (C.3, C.4, C.6) and PectGel3 (D3, D.4, D.6) woodpile structures after bioprinting (A.3, B.3, C.3, D.3), after freeze-drying (A.5, B.5, C.5, D.5) and after rehydration (A.6, B.6, C.6, D.6). SEM images with top view of freeze-dried Pect (A.5), PectGel1 (B.5), PectGel2 (C.5), and PectGel3 (D.5) woodpile structures (Scale bars A.2, B.2, C.2, D.2 = 5mm; A.3–A6, B.3–B.6, C.3–C.6, D.3–D.6 = 500 µm).

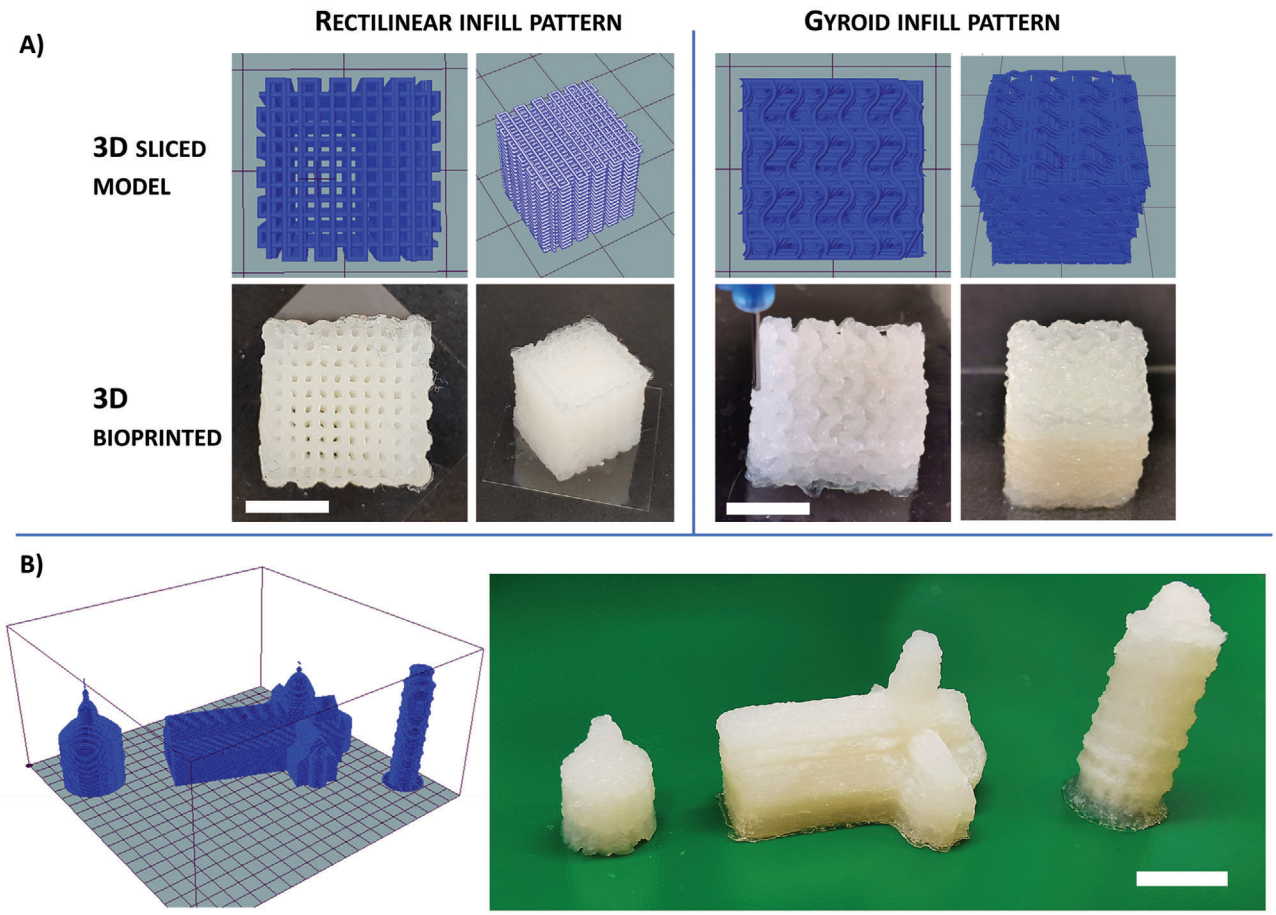

Figure 6. 3D scaffolds with different infill patterns, sizes and shapes obtained by 3D bioprinting PectGel3 biomaterial ink. Cubic shaped scaffolds (10 × 10 × 10 mm^3) with rectilinear infill pattern and gyroid infill pattern (Scale bar = 5 mm) (A), and a 3D sliced model and 3D bioprinted Piazza dei Miracoli of Pisa (leaning tower, Cathedral and Baptistery) (Scale factor 1:2000) (scale bar = 10 mm) (B).

both pectin and gelatin, up to 24 h for the PectGel3 formulation. This formulation, in fact, other than being ready-to-bioprint in a shorter time than the other PectGel formulations, allowed for longer bioprinting sessions. For these reasons, PectGel3 was selected to bioprint 3D scaffolds with different shapes and infill geometries to prove its bioprinting versatility (**Figure 6**). Large and complex shaped scaffolds were obtained without clogging the extrusion tip while bioprinting. Cubic shaped scaffolds 10 mm in height and with a rectilinear and gyroid infill patterns were successfully obtained (Figure 6A). Moreover, to demonstrate the shape retention capability of PectGel3 even in complexly shaped structures, a model of the Leaning Tower of Pisa together with the Cathedral and the Baptistery (scale factor 1:2000) was bioprinted (Figure 6B). It is important to mention that the entire bioprinting process occurred at ambient conditions without the use any additional heating/cooling device for the extruder and/or the printing plate.

3. Conclusion

This work reports on the preparation and characterization of biomaterial inks obtained by mixing pectin and gelatin crosslinked with GPTMS. The effects of gelatin content on porosity, pore size, water uptake and compressive modulus in dry and wet conditions were initially investigated on micro-porous, cylindrical sponges obtained by freeze-drying. Compared to Pect sponges, the addition of gelatin resulted in a decrease in porosity and water uptake. Moreover, a decrease of the compressive modulus at low gelatin content was observed in dry and wet conditions, while sponges with the highest gelatin concentration resulted in the stiffest sponges in wet conditions. Preliminary investigation on the effect of gelatin in PectGel sponges on human MG-63 osteoblast-like cell adhesion, showed the presence of elongated and adherent cells on all PectGel sponges. Finally, the effect of gelatin on pectin bioprintability was studied. 3D self-standing woodpile structures with designed macro- and micropores in the bioprinted struts were successfully obtained with all PectGel formulations by combining extrusion-based bioprinting and freeze-drying. In particular, PectGel3 (with the highest gelatin content) demonstrated to be the most suitable formulation for bioprinting complex shaped scaffolds, due to its larger window of printability. To demonstrate the PectGel3 bioprinting performance, 3D scaffolds with diverse shapes, heights and infill patterns were successfully bioprinted.

Concluding, novel and bioprintable biomaterial formulations were developed by combining pectin and gelatin. The presented results show the great potential of these formulations to be used

as biomaterial inks for extrusion-based 3D bioprinting of complex shaped scaffolds for TE applications.

4. Experimental Section

Preparation of PectGel Microporous Sponges: Aqueous PectGel slurries were prepared using a similar approach described in the previous work.[3] PectGel slurries were obtained by mixing citrus pectin (Herbstreit & Fox, Classic CU 701, degree of esterification 36%, MW 100–400 kDa[26]) and gelatin (Sigma Aldrich, porcine Type A) in ultrapure water (Arium mini ultrapure Lab Water System, Sartorius) at the weight ratios indicated in Table 1. The slurries were initially stirred at 70 °C for 1 h until pectin and gelatin were fully and homogenously dissolved. The pH of the resulting slurries ranged between 3 and 4. Subsequently, GPTMS (Sigma Aldrich) was added to the slurries. In particular, 920 µL[3] and 368 µL[36] of GPTMS per pectin and gelatin gram were used, respectively. Notably, the volume of GPTMS used to crosslink pectin is the same that allows to obtain a 3D bioprintable formulation, as shown in the previous work.[3]

The slurries were stirred for 40 min and subsequently poured into cylindrical molds (13 mm diameter × 10 mm height) to obtain cylindrical samples. These samples were initially frozen at −20 °C overnight to induce ice crystal formation, and subsequently freeze-dried (BenchTop Pro-SP Scientific) at −60 °C for 24 h to obtain microporous sponges. Once freeze-dried, the sponges were left to dry at 40 °C to induce the completion of pectin-gelatin-GPTMS reaction. GPTMS-crosslinked pectin sponges (without gelatin) (Table 1) were also produced and tested as control.

Physicochemical Characterization of PectGel Formulations and Sponges: The chemical composition of PectGel sponges was investigated through ATR-IR (Perkim-Elmer Spectrum Two) in the range of 400–4000 cm^{-1} with the resolution of 4 cm^{-1}. Dry solvent casted films made of PectGel1, PectGel2, PectGel3 were prepared on purpose for this analysis. These films were obtained by pouring the PectGel formulations (Table 1) in Petri dishes (≈5 mL in a 50 mm diameter Petri dish) and leaving them to dry on a heated plate at 40 °C until complete evaporation of the solvent (≈48 h). The ATR-IR spectra of raw GPTMS, and Pect films were also acquired as control. Moreover, crosslinked gelatin films, without pectin, were also obtained by solvent casting using a water-based gelatin solution (5% w/v) with GPTMS (368 µL per gelatin gram, named as GEL).

The morphology and architecture of micropores in the PectGel sponges was observed under a scanning electron microscope (Philips XL 20 SEM – FEI Italia SRL). Before SEM investigation, all sponges ($n = 3$) were sputter-coated with gold (Edwards Sputter Coater B150S equipment). The mean pore diameter of at least 70 micropores was measured from SEM images ($n = 3$) using Image J software.

The porosity of each sponge ($n = 3$) was determined gravimetrically by applying Equation (1).

$$\text{Porosity } [\%] = \left(1 - \frac{m_s}{\rho_{PectGel} V_s}\right) \times 100 \quad (1)$$

In Equation (1), m_s is the mass of each PectGel sponge (g), and V_s is the volume (cm^3) of each PectGel sponge measured with a caliper. Furthermore, $\rho_{PectGel}$ is the theoretical density (g cm^{-3}) of PectGel1, PectGel2, and PectGel3, respectively.[3] This parameter was calculated by ratio of the mass to volume of disk-shaped non-porous films ($n = 10$, Ø = 5 mm, 160 µm thick) obtained by solvent casting as above reported for the ATR-IR analysis.

The effect of gelatin on water uptake was investigated by immersing PectGel sponges in ultrapure water at 37 °C. The percentage of water uptake was measured after 30 min, 1 h, 2 h, 4 h, 24 h, 48 h, and 72 h by applying Equation (2).

$$\text{Water uptake } [\%] = \frac{W_s - W_0}{W_0} \times 100 \quad (2)$$

In Equation (2), W_0 is the initial weight (g) of dry PectGel sponges and W_S is the weight of hydrated sponges at different time points.

Uniaxial compressive tests were carried out to assess the effects of gelatin content on the stiffness of PectGel sponges both on the dry and wet state ($n = 5$). Hydrated sponges were incubated in ultrapure water at 37 °C until equilibrium of water uptake was reached. These experiments were performed on a Z005 series Zwick/Roell uniaxial compressive machine using a 100 N load cell, a strain rate of 1% s^{-1} and a maximum strain of 30%. The compressive modulus was finally calculated as the slope of the initial linear region (strain values between 1 and 7%) in the derived engineering stress–strain curves.

Cytocompatibility Investigation: Human MG-63 osteoblast-like cells (ATCC, Manassas) were cultured in Dulbecco Modified Eagle's Medium (H-DMEM, Corning Inc.) supplemented with 1% penicillin–streptomycin (Thermo Fisher Scientific) and 10% fetal bovine serum (Corning Inc.), and were incubated at 37 °C in a humidified atmosphere with 5% CO_2.

Prior to cell seeding, PectGel sponges (Ø = 5 mm, thickness = 3 mm, $n = 3$) were sterilized in ethanol 70% for 20 min, followed by UV exposure (30 min per side) and finally washed in Phosphate Buffer Solution (PBS, Sigma Aldrich).[3] The sponges were therefore placed in 48-well culture plates and preconditioned overnight in a complete H-DMEM without phenol red (Corning Inc.), and supplemented as previously described. MG-63 cells were subsequently seeded on the top of each sponge (2×10^4 cells per sponge), and the cell-seeded sponges were kept at 37 °C in a humidified incubator with 5% CO_2.

Cell viability of MG-63 cells on PectGel sponges at 48 h was measured using an XTT assay (Roche) according to the manufacturer's instructions. The XTT labelling medium was added to the cell culture medium (1:2 ratio) and the sponges were incubated at 37 °C for 4 h in darkness. Then, the absorbance of the medium was quantified by spectrophotometry (MultiskanGo, Thermo Scientific) at 555 nm with a reference wavelength at 655 nm. Cell viability of MG-63 on PectGel sponges was quantified as percentage of that of Pect sponges (control).

Finally, the morphology of MG-63 cells on PectGel sponges at 48 h was assessed by SEM. To this aim, seeded PectGel sponges ($n = 2$) were initially fixed in 0.1 M sodium cacodylate buffer (Sigma Aldrich) containing 2% glutaraldehyde (Merck), and subsequently washed with 0.1 M cacodylate buffer (containing 7% sucrose), and 0.1 M sodium cacodylate buffer (containing 1% osmium tetroxide) (Electron Microscopy Sciences). The seeded sponges were completely dehydrated by graded ethanol of 25, 50, 70, 80, 95, and 100%, and the critical point drying was performed with hexamethyldisilane (Sigma Aldrich). The sponges were therefore sputter-coated with gold using an Edwards Sputter Coater B150S, and analyzed using a Philips XL 20 SEM (FEI Italia SRL) microscope.

Extrusion-Based Bioprinting of PectGel Biomaterial Inks: Prior to bioprinting, each PectGel formulation (Table 1) was further stirred at 70 °C in order to induce an increase in viscosity due to the reaction between GPTMS and pectin-gelatin. This increment of viscosity is necessary to obtain self-supported 3D bioprinted scaffolds with high shape fidelity. When a visible increment of viscosity was observed (Table 3), the warm pectin-gelatin formulations (namely "biomaterial inks") were immediately loaded into the printer cartridge (a 5 mL syringe) with a spatula. Subsequently, they were cooled down to room temperature (25 °C) before starting to bioprint.

To assess the capability of shape retention after extrusion, 3D woodpile scaffolds 10 × 10 × 3.25 mm^3) (**Figure 7**) with a layer height of 250 µm were produced. A customized extrusion-based 3D bioprinter was used for these experiments[37] with a 22 G (410 µm inner diameter) straight extrusion tip. The bioprinting process was optimized by identifying the optimal printing speeds and flow rates for each biomaterial ink composition. These parameters are summarized in Table 3. Once bioprinted, the woodpile scaffolds were frozen at −20 °C, and freeze-dried at −60 °C as above described. Finally, the scaffolds were left on a heating plate at 37 °C for 4 days for completing the GPTMS cross-linking reaction.

Freeze-dried woodpile scaffolds were incubated in ultrapure water at 37 °C for 24 h in order to investigate the effect of rehydration on the scaffold's shape fidelity and structural stability. Finally, as-bioprinted, freeze-dried and rehydrated woodpile scaffolds were imaged using an optical microscope (Olympus AX 70), and the size of macropores and the line width was measured on 3 images using ImageJ software. The presence of

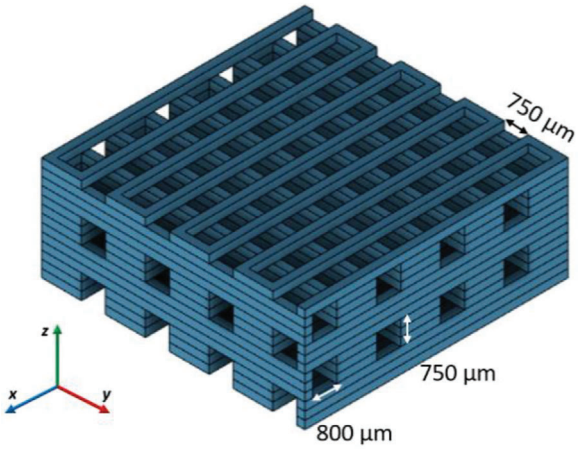

Figure 7. Illustration of the main features of the 3D bioprinted woodpile scaffold.

micropores within the bioprinted struts was additionally investigated through SEM images that were acquired with the above-described settings.

Additional bioprinting experiments were executed to test the capability of the developed PectGel biomaterial inks to bioprint scaffolds with different heights, surface area and infill pattern (such as gyroid infill pattern). To demonstrate the capability of PectGel3 biomaterial ink to bioprint 3D complex shaped structures without collapsing, a model of the Leaning Tower of Pisa, Cathedral and Baptistery (scale factor 1:2000) was bioprinted.

Statistical Analysis: The results are shown as mean value ± standard deviation. Statistical significance was assessed by using a Student's t-test to compare the properties of Pect (controls) to the other PectGel formulations. A significance level of 0.05 was considered. The Pearson correlation coefficient (r) was used to evaluate a linear correlation between the biomaterial formulation and specific physical properties.

Supporting Information

Supporting Information is available from the Wiley Online Library or from the author.

Acknowledgements

The authors are grateful to Herbstreith & Fox (Neuenburg, Germany) for kindly providing the pectin used in this study.

Conflict of Interest

The authors declare no conflict of interest.

Data Availability Statement

Research data are not shared.

Keywords

3D bioprinting, biofabrication, gelatin, pectin, scaffolds, tissue engineering

Received: April 21, 2021
Revised: June 7, 2021
Published online:

[1] L. Moroni, T. Boland, J. A. Burdick, C. De Maria, B. Derby, G. Forgacs, J. Groll, Q. Li, J. Malda, V. A. Mironov, C. Mota, M. Nakamura, W. Shu, S. Takeuchi, T. B. F. Woodfield, T. Xu, J. J. Yoo, G. Vozzi, *Trends Biotechnol.* **2018**, *36*, 384.
[2] W. Sun, B. Starly, A. C. Daly, J. A. Burdick, J. Groll, G. Skeldon, W. Shu, Y. Sakai, M. Shinohara, M. Nishikawa, J. Jang, D.-W. Cho, M. Nie, S. Takeuchi, S. Ostrovidov, A. Khademhosseini, R. D. Kamm, V. Mironov, L. Moroni, I. T. Ozbolat, *Biofabrication* **2020**, *12*, 022002.
[3] A. Lapomarda, A. De Acutis, I. Chiesa, G. M. Fortunato, F. Montemurro, C. De Maria, M. Mattioli Belmonte, R. Gottardi, G. Vozzi, *Biomacromolecules* **2019**, *21*, 319.
[4] R. Levato, T. Jungst, R. G. Scheuring, T. Blunk, J. Groll, J. Malda, *Adv. Mater.* **2020**, *32*, 1906423.
[5] I. Chiesa, C. Ligorio, A. F. Bonatti, A. De Acutis, A. M. Smith, A. Saiani, G. Vozzi, C. De Maria, *Front. Med. Technol.* **2020**, *7*, 71.
[6] M. A. Geven, A. Lapomarda, O. Guillaume, C. M. Sprecher, D. Eglin, G. Vozzi, D. W. Grijpma, *Eur. Polym. J.* **2021**, *147*, 110335.
[7] N. Paxton, W. Smolan, T. Böck, F. Melchels, J. Groll, T. Jungst, *Biofabrication* **2017**, *9*, 044107.
[8] A. S. Hoffman, *Adv. Drug Deliv. Rev* **2012**, *64*, 18.
[9] L. Kangseok, C. Cha, *Macromol. Res.* **2020**, *28*, 689.
[10] D. Chimene, R. Kaunas, A. K. Gaharwar, *Adv. Mater.* **2020**, *32*, 1.
[11] A. I. Cernencu, A. Lungu, I.-C. Stancu, A. Serafim, E. Heggset, K. Syverud, H. Iovu, *Carbohyd. Polym* **2019**, *220*, 12.
[12] D. N. Heo, M. A. Alioglu, Y. Wu, V. Ozbolat, B. Ayan, M. Dey, Y. Kang, I. T. Ozbolat, *ACS Appl. Mater. Interfaces* **2020**, *12*, 20295.
[13] A. Leucht, A. - C. Volz, J. Rogal, K. Borchers, P. J. Kluger, *Sci. Rep.* **2020**, *10*, 1.
[14] M. Hospodiuk, M. Dey, D. Sosnoski, I. T. Ozbolat, *Biotechnol. Adv.* **2017**, *35*, 217.
[15] D. L. Johnson, R. M. Ziemba, J. H. Shebesta, J. C. Lipscomb, Y. Wang, Y. Wu, K. D. O'connell, M. G. Kaltchev, A. Van Groningen, J. Chen, X. Hua, W. Zhang, *Biomed. Phys. Eng. Express* **2019**, *5*, 067004.
[16] P. Sriamornsak, *S. Univ. Open J. Syst.* **2003**, *6*, 206.
[17] F. Munarin, M. C. Tanzi, P. Petrini, *Int. J. Biol. Macromol* **2012**, *51*, 681.
[18] M. Moslemi, *Carbohydr. Polym.* **2020**, 117324.
[19] G. E. D. O. Nascimento, F. F. Simas-Tosin, M. Iacomini, P. A. J. Gorin, L. M. C. Cordeiro, *Carbohydr. Polym.* **2016**, *139*, 125.
[20] K. Muhammad, N. I. Nur, S. P. Gannasin, N. Mohd Adzahan, J. Bakar, *Food Hydrocoll.* **2014**, *42*, 289.
[21] A. Hajikhani, F. Scocozza, M. Conti, M. Marino, F. Auricchio, P. Wriggers, *Int. J. Artif. Organs* **2019**, *42*, 548.
[22] J. A. Rowley, D. J. Mooney, *J. Biomed. Mater. Res.* **2002**, *60*, 217.
[23] R. K. Mishra, A. B. A. Majeed, A. K. Banthia, *Int. J. Plast. Technol.* **2011**, *15*, 82.
[24] T. B. L. Nguyen, Y. K. Min, B. T. Lee, *Tissue Eng. – Part A* **2015**, *21*, 1376.
[25] M. Tummalapalli, M. Berthet, B. Verrier, B. L. Deopura, M. S. Alam, B. Gupta, *Int. J. Biol. Macromol.* **2016**, *82*, 104.
[26] M. Saravanan, K. P. Rao, *Carbohydr. Polym.* **2010**, *80*, 808.
[27] S. Nejati, R. Karimi Soflou, S. Khorshidi, A. Karkhaneh, *Colloids Surf., B* **2020**, *196*, 111347.
[28] L. Ren, K. Tsuru, S. Hayakawa, A. Osaka, *J. Sol-Gel Sci. Technol.* **2001**, *21*, 115.
[29] C. Tonda-Turo, E. Cipriani, S. Gnavi, V. Chiono, C. Mattu, P. Gentile, I. Perroteau, M. Zanetti, G. Ciardelli, *Mater. Sci. Eng. C* **2013**, *33*, 2723.
[30] A. N.-C. Chao, *J. Memb. Sci.* **2008**, *311*, 306.
[31] V. B. V. Maciel, C. M. P. Yoshida, T. T. Franco, *Carbohydr. Polym.* **2015**, *132*, 537.
[32] J. H. Muyonga, C. G. B. Cole, K. G. Duodu, *Food Chem.* **2004**, *86*, 325.
[33] C. Tonda-Turo, P. Gentile, S. Saracino, V. Chiono, V. K. Nandagiri, G. Muzio, R. A. Canuto, G. Ciardelli, *Int. J. Biol. Macromol.* **2011**, *49*, 700.

[34] Q. L. Loh, C. Choong, *T. Eng. – Part B Rev* **2013**, *19*, 485.
[35] H. R. Moreira, F. Munarin, R. Gentilini, L. Visai, P. L. Granja, M. C. Tanzi, P. Petrini, *Carbohydr. Polym* **2014**, *103*, 339.
[36] G. M. Fortunato, F. Da Ros, S. Bisconti, A. De Acutis, F. Biagini, A. Lapomarda, C. Magliaro, C. De Maria, F. Montemurro, D. Bizzotto, P. Braghetta, G. Vozzi, *Front. Bioeng. Biotechnol.* **2019**, *7*, 174.
[37] I. Chiesa, G. M. Fortunato, A. Lapomarda, L. Di Pietro, F. Biagini, A. De Acutis, L. Bernazzani, M. R. Tinè, C. De Maria, G. Vozzi, *Int. J. Artif. Organ 42*, **2019**, 586.